RSC Advances

PAPER

View Article Online
View Journal | View Issue

Cite this: *RSC Adv.*, 2025, **15**, 16845

A systematic study of the NaMnAs half-Heusler compound from bulk to (001) surfaces as promising spintronic materials

Chu Viet Ha,[a] Somekeo Keovongsa,[a] Armando Reyes-Serrato,[b] J. Guerrero-Sanchez[b] and D. M. Hoat *[cd]

The search for new materials for practical implementation in spintronic devices has attracted enormous attention. In this work, the electronic and magnetic properties of half-Heusler NaMnAs alloy in its bulk conformation and as (001) surfaces are investigated using the full-potential linearized augmented plane wave (FP-LAPW) method. The bulk NaMnAs compound is a ferromagnetic spin-gapless semiconductor (SGS) material, whose total magnetic moment of 5.00μ_B per unit cell satisfies the Slater–Pauling rule and is produced mainly by Mn atoms. The SGS nature is retained with external tensile strain, meanwhile the transition to a magnetic semiconductor (MS) nature is achieved by compressive strain up to −6%. In addition, stronger compression applied to the lattice causes material metallization. Further, (001) surfaces with MnNa- and As-termination with different thickness (5ML, 7ML, 9ML, and 11ML) are considered. It is found that both spin states of MnNa-terminated surfaces exhibit a metallic character, while half-metallicity is observed for the As-terminated surfaces. The calculated projected density of states indicates a key role of As-p and Mn-d orbitals in regulating the electronic nature of both bulk and surface counterparts. Interestingly, except for 11ML-As-terminated surfaces, the out-of-plane easy spin magnetization is demonstrated through calculating the magnetic anisotropy energy. Our results may introduce the new half-Heusler NaMnAs compound for spintronic applications, providing insights into the change of electronic and magnetic properties from the bulk state to (001) surfaces.

Received 20th March 2025
Accepted 25th April 2025

DOI: 10.1039/d5ra01968k

rsc.li/rsc-advances

1. Introduction

The key role of physical properties of materials in developing the technological applications is well known. Spintronics is an emerging field that uses the spin of electrons to encode, process, and transport data rather than their charge.[1,2] In this regard, half-metallic (HM) materials form a fabulous family that has attracted special research interest because of their promise for device applications including spin injectors,[3,4] spin valves,[5,6] and magnetic tunnel junctions.[7,8] The concept of half-metallicity was proposed for the first time by de Groot *et al.*[9] when investigating the band structure of NiMnSb and PtMnSb half-Heusler compounds, whose band structures are composed of one metallic spin state and one semiconductor spin state to reach a 100% of spin polarization at the Fermi level. After that, researchers made efforts to confirm experimentally the half-metallicity.[10–12] Since then, studies have reported something closely related to HM materials, namely spin-gapless semiconductors (SGSs) that have a closed band gap in one spin channel (semimetal character) and open band gap in the other one (semiconductor character).[13,14] In SGS materials, both excited electrons and holes can be 100% spin-polarized, such that the magnetic state or external magnetic field can influence significantly their transport properties. The other feature-rich type of band structure is that both spin channels have an open band gap with significant magnetic moments, giving place to the formation of magnetic semiconductor (MS) materials.[15,16] Similar to HM materials, SGSs and MSs are interesting magnetic candidates to be employed in spintronic devices.[17–20]

In 1903, the first Heusler alloy Cu_2MnAl was discovered by Fritz Heusler – a German chemist and mining engineer. Interestingly, this compound exhibits ferromagnetism at room temperature despite none of its constituent elements (Cu, Mn, and Al) being ferromagnetic in their bulk state.[21] Since then, more than 1000 Heusler compounds have been investigated, including full-Heusler compounds with 2 : 1 : 1 stoiquiometry,[22,23] half-Heusler compounds with 1 : 1 : 1 stoiquiometry,[24,25] and the recently investigated equiatomic quaternary Heusler (EQH) compounds with 1 : 1 : 1 : 1 stoiquiometry.[26,27] Normally, Heusler compounds crystallize in a cubic crystal structure, in

[a]*Faculty of Physics, TNU-University of Education, Thai Nguyen, 250000, Vietnam*
[b]*Universidad Nacional Autónoma de México, Centro de Nanociencias y Nanotecnología, Apartado Postal 14, Ensenada, Baja California, Código Postal 22800, Mexico*
[c]*Institute of Theoretical and Applied Research, Duy Tan University, Ha Noi 100000, Vietnam. E-mail: dominhhoat@duytan.edu.vn*
[d]*Faculty of Natural Sciences, Duy Tan University, Da Nang 550000, Vietnam*

which the constituent atoms of full-Heusler and EQH alloys occupy the high-symmetry Wyckoff 4a, 4b, 4c, and 4d positions. When one of the mentioned sublattices is empty, the half-Heusler compound is formed. Extensive investigations have demonstrated diverse extraordinary properties of Heusler compounds including half-metallicity, magnetic semiconducting, spin-gapless semiconducting, nonmagnetic semiconducting, and superconducting,[28–30] among others.

Because of their structural versatility, the design of Heusler compounds can be realized by varying the chemical composition. Recently, we have designed half-Heusler alloys based on Na–TM–VA elements (TM = 3d transition metals and VA = pnictogen atoms) using first-principles calculations.[31,32] It is found that Na, TM, and VA atoms prefer to occupy 4c, 4d, and 4a positions, respectively. Moreover, the physical properties depend strongly on the nature of the TM and VA atoms. On the other hand, the study of multilayers or thin films of Heusler compounds is necessary for practical spintronic applications since the material properties may change significantly from bulk counterparts to surfaces. For example, the half-metallic characteristic in bulk Mn_2CoSn is lost at (001) surfaces regardless of the surface termination.[33] The half-metallicity is also observed in bulk Mn_2CoAl that is retained in the AlMn-terminated (001) surfaces, meanwhile this feature is destroyed in the CoMn-terminated (001) surfaces.[34]

In this work, we investigate the electronic and magnetic properties of bulk NaMnAs Heusler compound and its (001) surfaces. It is anticipated that in its bulk counterpart, this compound is a spin-gapless semiconductor. Upon forming (001) surfaces, different features are obtained. Specifically, the metallic nature is observed for the MnAs-terminated surfaces, while the half-metallicity is obtained with As-termination. The results may recommend this new half-Heusler alloy for spintronic applications.

2. Computational details

Using the approach of density functional theory (DFT),[35] theoretical calculations are performed *via* WIEN2k code[36] using the full-potential linearized augmented plane wave (FP-LAPW) method. A separation energy of −6.0 Ry is set to separate valence states from core states. The generalized gradient approximation is employed to consider the electron exchange–correlation interactions, where the Perdew–Burke–Ernzerhof (GGA-PBE) version is adopted.[37] In addition, highly correlated Mn-3d electrons are also treated with the PBE+U method[38] using an effective Hurbbard parameter of $U_{\text{eff}} = 6.0$ eV.[39,40] The cut-off parameter is set to $R_{\text{MT}} \times K_{\text{max}} = 8$, where R_{MT} and K_{max} denote the smallest radius of atomic spheres and the maximum value of the reciprocal lattice vectors, respectively. Within the muffin-tin (MT) spheres the highest angular momentum of $l_{\text{max}} = 10$ is set, while the expansion of charge density and potential in the interstitial region is realized with wave vectors up to $G_{\text{max}} = 12$. The self-consistent DFT calculations are iterated with a convergence criterion of 0.0001 Ry. Structural relaxation is carried out with a criterion of residual force set to be 0.5 mRy Bohr^{-1}. k-Point grids of 10 × 10 × 10 and 8 × 8 × 2 are employed to sample the Brillouin zone of the cubic bulk phase and (001) surfaces of the NaMnAs half-Heusler compound. In the slab models, a vacuum is inserted with thickness of 15 Å to minimize the inter-slab interactions.

3. Results and discussion

3.1. Bulk NaMnAs half-Heusler compound

The NaMnAs half Heusler compound adopts a cubic structure belonging to $F\bar{4}3m$ space group as displayed in Fig. 1a. There are four formula unit in the unit cell, in which the Na, Mn, and As atoms are situated at 4c(0.25, 0.25, 0.25), 4d(0.75, 0.75, 0.75), and 4a(0.0, 0.0, 0.0) Wyckoff positions, respectively. As a first step of investigation, the system energy is calculated at various volumes for nonmagnetic (NM), antiferromagnetic (AFM), and ferromagnetic (FM) states. Results plotted in Fig. 1b show that the FM state has lower energy than NM and AFM state, confirming the stabilization of the FM state in the studied NaMnAs half-Heusler compound. The Birch–Murnaghan equation of

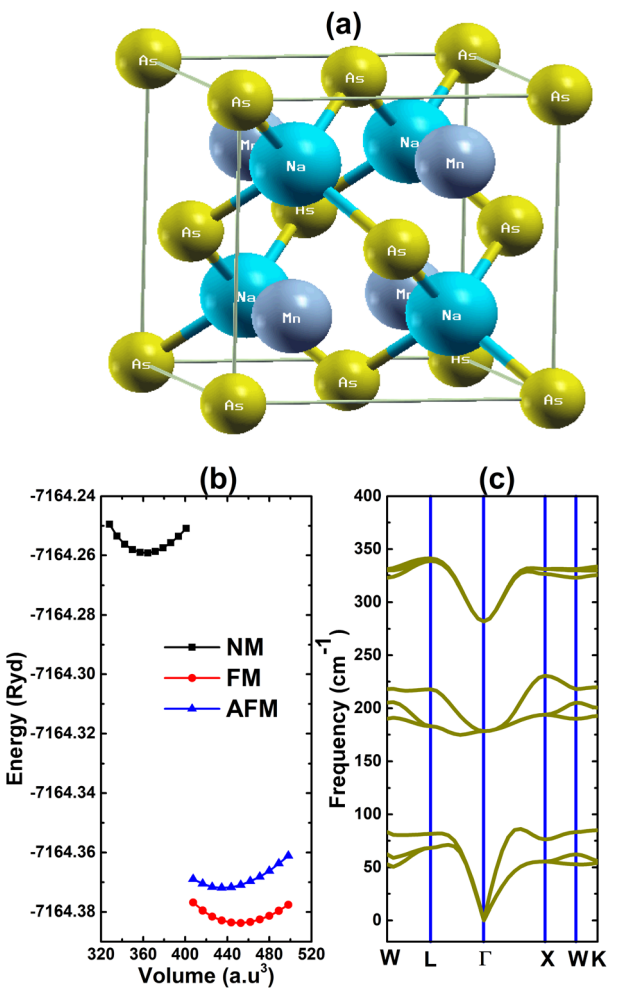

Fig. 1 (a) Atomic structure in a unit cell, (b) energy as a function of volume for nonmagnetic (NM), antiferromagnetic (AFM), and ferromagnetic (FM) states, and (c) phonon dispersion curves of the NaMnAs half-Heusler compound.

state is employed to represent the energy–volume relation as follows:[41]

$$E(V) = E_0 + \frac{9V_0B}{16}\left\{\left[\left(\frac{V_0}{V}\right)^{2/3} - 1\right]^3 B' + \left[\left(\frac{V_0}{V}\right)^{2/3} - 1\right]^2\left[6 - 4\left(\frac{V_0}{V}\right)^{2/3}\right]\right\} \quad (1)$$

where V_0 = initial volume; V = deformed volume; B = bulk modulus; and B' = derivative of the bulk modulus. The optimal lattice constant is determined through minimizing the energy as a function of volume. Our calculations provide a lattice constant of 6.44 Å for the NaMnAs half-Heusler compound that will be used for further investigating its electronic and magnetic properties. In order to verify the structural stability of the NaMnAs half-Heusler compound, its phonon dispersion curves are calculated using the finite displacement method as implemented in the PHONOPY code.[42] From Fig. 1c, one can see nine phonon modes for any chosen p point that are derived from vibration of three atoms (one unit formula – NaMnAs) in a primitive cell. Importantly, the absence of any imaginary mode confirms that the NaMnAs half-Heusler compound is dynamically stable.

Fig. 2a shows the spin-polarized band structure of the NaMnAs alloy along W–L–Γ–X–W–K path in the irreducible Brillouin zone. The band structure profile indicates the semimetal character of the spin-up state, where the valence band maximum (VBM) and conduction band minimum (CBM) touch at the Fermi level. In addition, there is an indirect gap of 1.91 eV for spin-down state that is formed by the separation between the VBM point at the Γ point (energy of −1.21 eV) and the CBM point at the X point (energy of 0.70 eV). The results mean that the ternary NaMnAs Heusler compound is a spin-gapless semiconductor material, which is suitable for spintronic applications. The projected density of states (PDOS) of this alloy is given in Fig. 2b. PDOS values demonstrate the small contribution of the Na atom to the formation of the band structure. The valence band is formed mainly by the As-p orbital, while Mn-d_{eg}–$d_{t_{2g}}$ states and As-p states originate mainly in the conduction band (of spin-down and spin-up channels, respectively).

Now, we assess the effects of external strain on the electronic band structure of the NaMnAs half-Heusler compound, which is defined through lattice constant as follows: $\varepsilon = \frac{a_s - a_e}{a_e} \times 100\%$, where a_s and a_e denote the lattice constant at strained and equilibrium conditions, respectively. Fig. 3 shows the edge energies of the considered bulk material at different strains. Note that the spin-gapless semiconductor nature is retained when applying the lattice expansion, however the spin-down band gap is reduced such that both VBM and CBM points shift towards the Fermi level. The transition of electronic nature is induced when applying the lattice contraction. Specifically, the spin-up band gap is opened and the spin-down semiconductor character is preserved upon compressive strain up to −6%, demonstrating the transition from a spin-gapless semiconductor nature to magnetic semiconductor nature. Stronger lattice compression will metallize the material since the metallic character is observed for both spin states from a compressive strain of −7%.

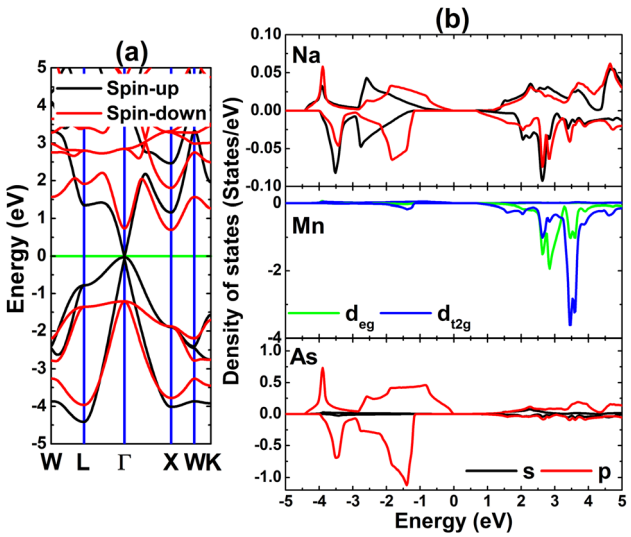

Fig. 2 (a) Spin-polarized band structure (green line: the Fermi level is set to 0 eV) and (b) projected density of states of the NaMnAs half-Huesler compound.

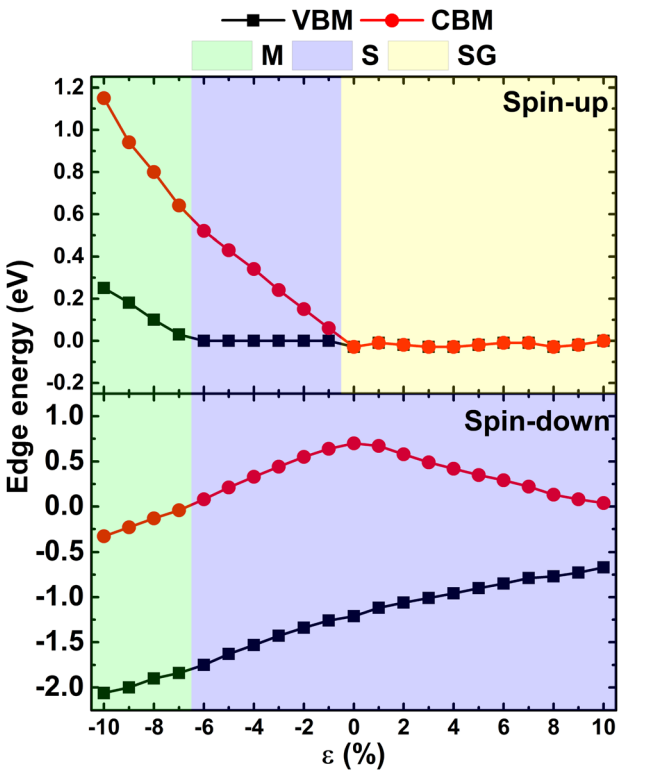

Fig. 3 Band edges and electronic nature (M: metallic; S: semiconductor; SG: spin-gapless) of the NaMnAs half-Heusler compound under effects of external strain.

Importantly, the magnetism of the NaMnAs half-Heusler compound is confirmed by its significant magnetic moments. The total magnetic moment has four components: (1) an interstitial magnetic moment of $0.28\mu_B$; (2) a local magnetic moment of the Na atom of $0.00\mu_B$; (3) a local magnetic moment of the Mn atom of $4.76\mu_B$; and (4) a local magnetic moment of the As atom of $-0.04\mu_B$. Consequently, an integer value of $5.00\mu_B$ is obtained. Note that this result follows the Slater–Pauling rule that defines the relation between total magnetic moment M_t and total valence electrons Z_t as follows:[43] $M_t = Z_t - 8$. The considered material has 13 valence electrons (1 valence electron of the Na atom + 7 valence electrons of the Mn atom + 5 valence electrons of the As atom). These results indicate that the magnetism of the NaMnAs alloy originates primarily from the Mn atom. This feature is further confirmed by the spin density in a unit cell illustrated in Fig. 4a. Note that spin surfaces are centered mainly at the Mn sites, indicating the key role of this transition metal in the origin of the material's magnetic moment. Furthermore, the total magnetic moments and local magnetic moment of the Mn atoms under the effects of external strain are investigated. From Fig. 4b, it can be seen that total magnetic moment only decreases slightly with compressive strain from −9%, while the magnetic moment of the Mn atom increases slightly from lattice compression to lattice expansion. These findings suggest the robustness of ferromagnetism in the NaMnAs half-Heusler compound under the influence of external strain.

As an essential parameter of ferromagnetic materials, the Curie temperature T_C of the NaMnAs compound is estimated using the relation with total magnetic moment M_t as follows [44]

$$T_C = 23 + 181 \times M_t \quad (2)$$

With a total magnetic moment of $5.00\mu_B$, the studied half-Heusler compound has a Curie temperature of 928 K, which is comparable with other half-Heusler compounds.[45]

3.2. (001) surfaces of NaMnAs half-Heusler compound

In this part, the NaMnAs half-Heusler compound is simulated as a thin film to examine the variation of electronic and magnetic properties from the bulk to surface counterparts, which is necessary to recommend new materials for practical implementation in spintronic devices. Along the [001] direction, the structure is formed by alternating atomic layers that allows the cleaving of (001) surfaces with two kinds of terminations, namely MnNa-terminated and As-terminated (001) surfaces. In addition, slabs with five, seven, nine, and eleven atomic monolayers (denoted by 5ML, 7ML, 9ML, and 11ML,

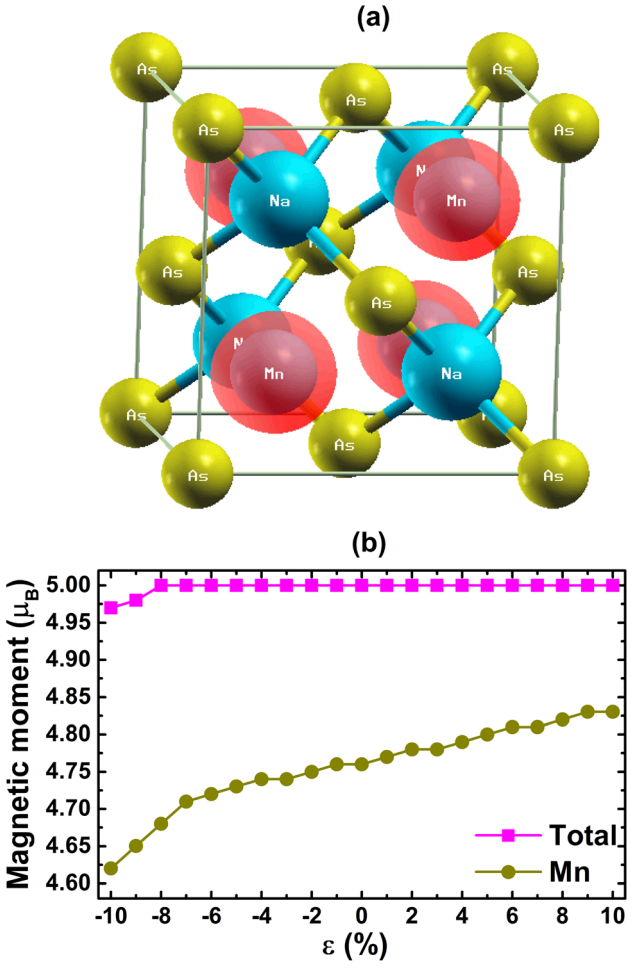

Fig. 4 (a) Spin density (iso-surface value: 0.1 e Å^{-3}) at an unstrained state and (b) total magnetic moment of the NaMnAs half-Heusler compound and local magnetic moment of the Mn atom under the effects of external strain.

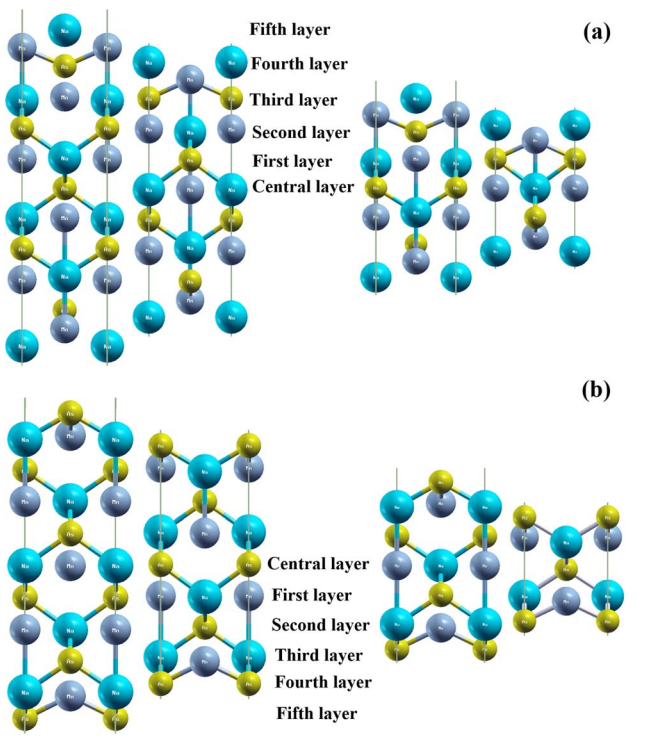

Fig. 5 Atomic structure of (a) MnNa- and (b) As-terminated (001) surfaces of NaMnAs half-Heusler compounds with different thicknesses (from the left to the right: 11ML-9ML-7ML-5ML).

Table 1 Atomic displacements (Å) of NaMnAs (001) surfaces with different thicknesses (positive value: outward movement; negative value: inward movement)

		MnNa-terminated				As-terminated			
Layer	Atom	5ML	7ML	9ML	11ML	5ML	7ML	9ML	11ML
1st	Na	—	−0.168	—	+0.022	−0.149	—	+0.040	—
	Mn	—	+0.095	—	−0.040	+0.122	—	−0.012	—
	As	+0.078	—	−0.003	—	—	−0.048	—	−0.003
2nd	Na	+0.385	—	−0.143	—	—	−0.112	—	+0.024
	Mn	−0.475	—	+0.033	—	—	+0.083	—	+0.001
	As	—	+0.062	—	+0.001	−0.415	—	−0.021	—
3rd	Na	—	+0.382	—	−0.142	—	—	−0.101	—
	Mn	—	−0.560	—	+0.051	—	—	+0.115	—
	As	—	—	+0.068	—	—	−0.406	—	−0.034
4th	Na	—	—	+0.368	—	—	—	—	−0.095
	Mn	—	—	−0.543	—	—	—	—	+0.106
	As	—	—	—	+0.076	—	—	−0.381	—
5th	Na	—	—	—	+0.385	—	—	—	—
	Mn	—	—	—	−0.533	—	—	—	—
	As	—	—	—	—	—	—	—	−0.385

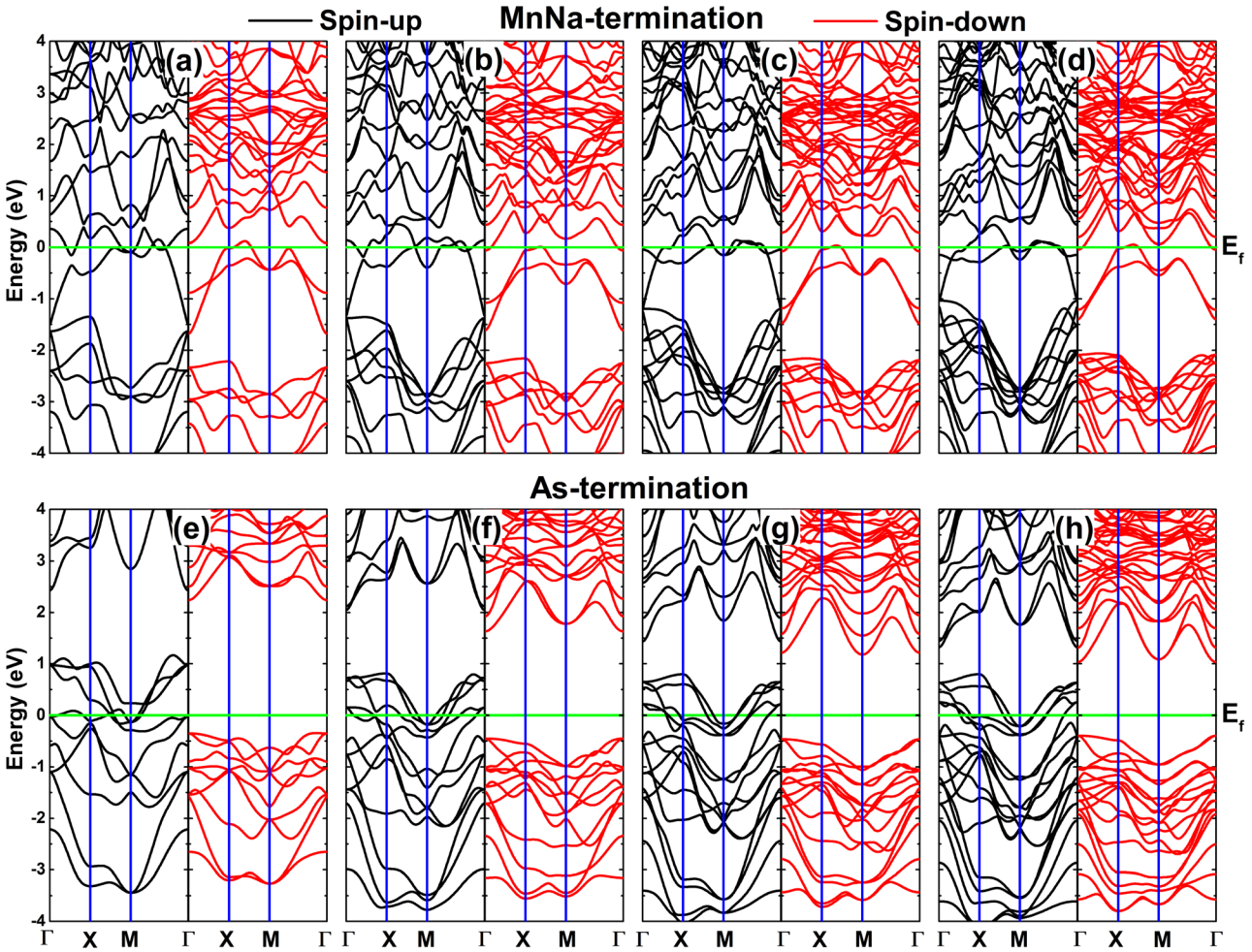

Fig. 6 Spin-polarized band structure of (001) surfaces of the NaMnAs half-Heusler compound with (a and e) 5ML, (b and f) 7ML, (c and g) 9ML, and (d and h) 11ML of thickness.

respectively) are considered to also investigate the effects of slab thickness. We employ the equilibrium lattice constant (6.44 Å) of bulk NaMnAs to construct its (001) surfaces, and the equilibrium surface structures are obtained by allowing all the constituent atoms to relax freely. Fig. 5 shows the atomic structures after relaxation, in which the names of the layers are also indicated. Regardless of the surface termination, it is found that the atoms in the central layer do not move from their original position, meanwhile those in other layers exhibit vertical displacement (displacing only along the *z*-direction). Specifically, our analysis implies an inward movement for Na and As atoms, meanwhile Mn atoms show an outward movement. The displacements of constituent atoms from their original positions are listed in Table 1. Note that the displacement is considerably larger in MnNa-layers than in As-layers. Moreover, as a general trend, the movement magnitude increases from internal layers to outside layers. Our calculations show only perpendicular movement, where no apparent surface reconstruction is observed. This is a general tend of the (001) surface of Heusler compounds.[46]

The spin-polarized band structures of (001) surfaces of the NaMnAs alloy are given in Fig. 6, which exhibit novel electronic features different from that of the bulk counterpart. It is found that both spin states of the MnNa-terminated surfaces have a metallic character regardless of the surface thickness, indicating the material metallization induced by the surface cleavage. Meanwhile, half-metallicity is observed for all the As-terminated surfaces considering their spin-up metallic state and semiconductor spin-down state. It appears that the slab thickness does not influence the half-metallic nature, however the conduction band shifts towards the Fermi level when increasing the number of layers. Specifically, our analysis indicates the CBM point located at energies of 2.24, 1.63, 1.18, and 1.03 eV for 5ML, 7Ml, 9ML, and 11ML surfaces, respectively.

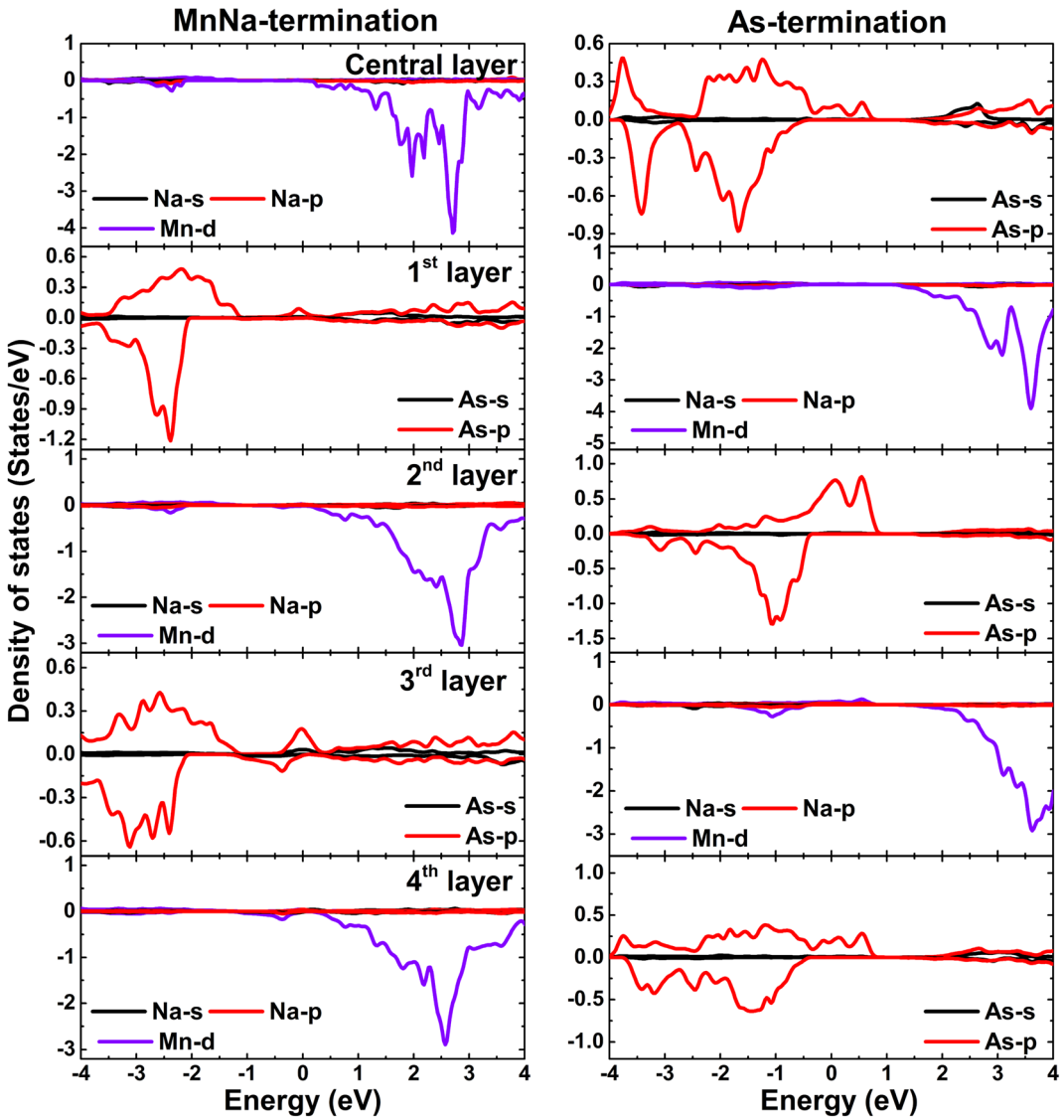

Fig. 7 Layer-separated projected density of states of MnNa- and As-terminated (001) surfaces of the NaMnAs half-Heusler compound with 9ML thickness.

Moreover, the VBM points are found at −0.34, −0.45, −0.46, and −0.39 eV, respectively. Consequently, spin-down energy gaps of 2.58, 2.08, 1.64, and 1.42 eV are obtained, respectively. Note that this parameter increases when thinning the As-terminated (001) surface. It is important to mention that the half-metallic gap is an essential parameter of half-metallic materials, which is defined as the smaller distance between the conduction band minimum and valence band maximum with respect to the Fermi level.[47,48] Considering the definition, half-metallic gaps of 0.34, 0.45, 0.46, and 0.39 eV are obtained for As-terminated (001) surfaces of the NaMnAs half-Heusler compound with thicknesses of 5ML, 7ML, 9ML, and 11ML, respectively. These large values suggest the robustness of the half-metallicity of As-terminated (001) surfaces under the influence of external factors.

As a representative example, the PDOS spectra of MnNa-terminated and As-terminated (001) surfaces with 9ML thickness are given in Fig. 7 to investigate the band structure formation. Note that the contribution from the Na atom is quite small – a feature that is similar to that in bulk counterpart. Importantly, the spin-up and spin-down metallic character of the MnNa-terminated slab can be attributed to the As-p state or Mn-d state, respectively, and mostly to those atoms of outside layers – that is "surface states". In other words, the As-p state is mainly responsible for the spin-up metallic behavior in the case of As-termination, while the spin-down energy gap is formed by the separation between the As-p state at the upper part of the valence band and the Mn-d state at the lower part of the conduction band.

Now, we turn to the investigation of the magnetism in NaMnAs (001) surfaces. According to our calculations, total magnetic moments of 14.12, 18.98, 21.98, and 29.04μ_B are obtained for MnNa-terminated surfaces with 5ML, 7ML, 9ML, and 11ML thickness, respectively. Meanwhile, integer values of 7.00 > 12.00 > 17.00 > 22.00 are obtained for the half-metallic As-terminated surfaces when increasing the surface thickness in the direction 5ML > 7ML > 9ML > 11ML. Fig. 8 shows the spin density to clarify the origin of magnetic moments in the considered slabs (thickness 9ML is chosen as a representative). From the figure, one can conclude that the magnetic moments are produced mainly by Mn atoms. It is important to note a small contribution from the outermost As atoms in the case of As-terminated surfaces, which exhibit antiparallel spin coupling to Mn atoms.

Since Mn atoms mainly produce the magnetism of the surfaces with both terminations, local magnetic moments of this transition metal at different layers are given in Fig. 9. From the figure, one can see that this parameter decreases slightly from internal to outside layers. This feature is a result of the increasing interactions between Mn and As atoms considering the opposite relaxations of these atoms, that is they move close to each other.

Finally, we examine the magnetic anisotropy of NaMnAs (001) surfaces through calculating the magnetic anisotropy energy (MAE) using the force theorem approach that comprises of two steps: (1) self-consistent calculations without spin–orbit coupling (SOC) followed by (2) SOC calculations with in-plane axis [001] and out-of-plane axis [100] spin magnetization using self-consistent charge density as an input. Then the MAE is defined by: MAE = E[001] − E[100]. It is found that except for the

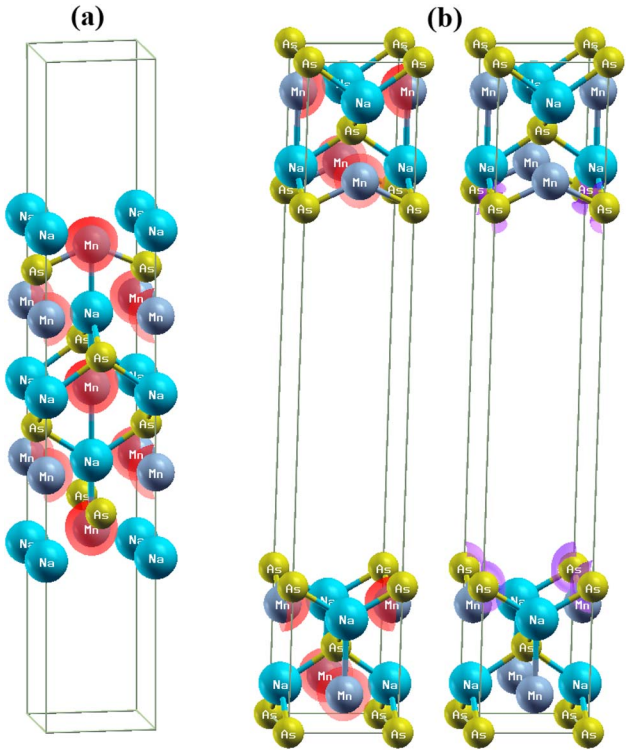

Fig. 8 Spin density (iso-surface value: 0.1 e Å^{-3}; red surface: spin-up; violet surface: spin-down) in (a) MnNa- and (b) As-terminated (001) surface of the NaMnAs half-Heusler compound with 9ML thickness.

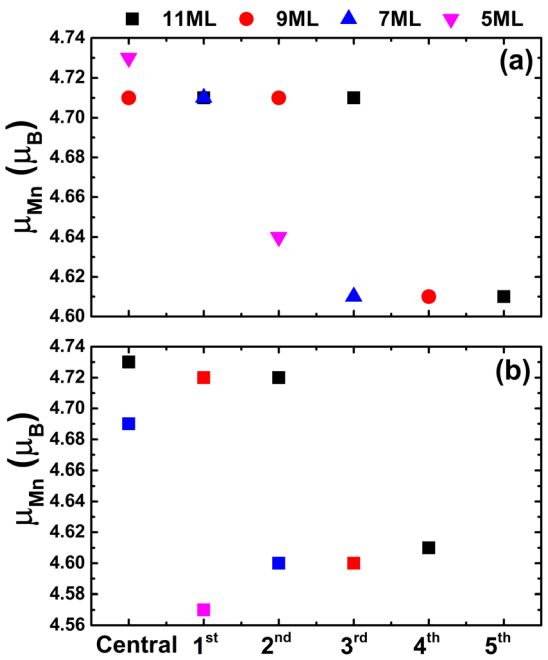

Fig. 9 Local magnetic moment of Mn atoms in different layers of (a) MnNa- and (b) As-terminated (001) surfaces of the NaMnAs half-Heusler compound with 11ML, 9ML, 7ML, and 5ML thickness.

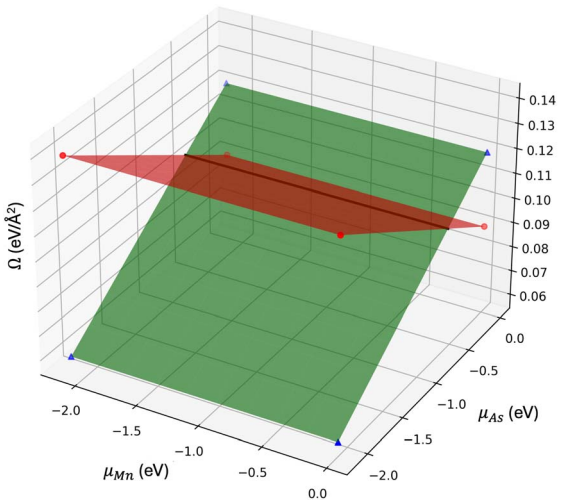

Fig. 10 Surface formation energy (Ω) *vs.* μ_{Mn} and μ_{As} chemical potentials in eV Å^{-2} (green plane represents the MnNa-terminated surface and the red one defines the As-terminated surface; black line in the stability map defines the region where the stability change happens).

As-terminated slab with 11ML of thickness that has in-plane easy magnetization with an MAE value of +6.39 eV, an out-of-plane (along *z*-axis) easy magnetization is obtained in the remaining cases. Specifically, MnNa-terminated surfaces with 5ML/7ML/9ML/11ML thicknesses and As-terminated surfaces with 5ML/7ML/9ML thicknesses have MAE values of −3.48/−5.77/−4.72/−3.50 and −0.41/−1.75/−1.75 meV, respectively. Since NaMnAs (001) surfaces with As-termination (5ML, 7ML, and 9ML of thickness) are half-metallic with perpendicular magnetic anisotropy, they are highly recommended for spin injection and the construction of magnetic spin junctions.

3.2.1. Thermodynamic stability. Once we studied the different surface terminations of the half-Heusler NaMnAs alloy, we determined their relative stability compared to the bulk NaMnAs. A perfect tool to do that is the surface formation energy (Ω). This approximation considers a surface in equilibrium with the bulk and its surroundings so they can exchange atoms.[49] The chemical potential is the way to measure the changes in energy due to these atomic exchanges. Following the procedure described by Moreno-Armenta *et al.*,[50] the surface formation energy used in this work is:

$$\Omega = \frac{1}{2A}\left[E_{\text{slab}} - n_{\text{Na}}\mu^{\text{Bulk}}_{\text{NaMnAs}} - \mu_{\text{Mn}}(n_{\text{Mn}} - n_{\text{Na}}) - \mu_{\text{As}}(n_{\text{As}} - n_{\text{Na}})\right] \quad (3)$$

where E_{slab} stands for the energy of the different surfaces, $\mu^{\text{Bulk}}_{\text{NaMnAs}}$ is the chemical potential of the half-Heusler NaMnAs alloy, μ_{Mn} and μ_{As} define the chemical potential of Mn and As atoms, respectively. Also, n_i is the number of atoms of each species. Finally, A is the surface area in Å^2. Ω is usually evaluated in different growth ranges, defined by the formation enthalpy of the treated compound $\Delta H_f^{\text{NaMnAs}} = 2.13$ eV per unit formula. Considering that, the growth ranges are then defined as $-\Delta H_f^{\text{NaMnAs}} \leq \mu_i \leq 0$, for each of the dependent Mn and As variables. Considering that, we end up plotting stability planes in the chemical potential domain.

Upon analyzing the results depicted in Fig. 10, it is possible to observe that both surfaces, As-terminated and MnNa-terminated, are stable at different growth ranges. Stability in this formalism is related to the zones with the lowest formation energies. Notice from the figure that at all Mn growth conditions and As-poor conditions, the most stable structure is the MnNa-terminated surface. Upon increasing the As content and reaching almost an As-rich environment, the stability trend changes, and the stable surface termination is now the As-terminated. Also, we determined the region in which the stability trend changes so that the stability passes from the MnNa-terminated to the As-terminated surface, which is $\mu_{\text{As}} = -0.58$ eV; such a value confirms that the stability of the As-terminated surface is at the zone of As-rich conditions.

4. Conclusions

In summary, FL-LAPW calculations have been carried out to investigate the electronic and magnetic properties of bulk and (001) surfaces of the NaMnAs compound. The dynamical stability of this half-Heusler alloy is confirmed by phonon dispersion curves. The spin-polarized band structure indicates its spin-gapless semiconductor nature that is preserved upon applying tensile strain. Meanwhile compressive strain leads to a state transition in the direction: spin-gapless semiconductor > half-metallic > metallic. The total magnetic moment exhibits negligible variation, meanwhile the local magnetic moment of Mn atoms increases slightly from lattice compression to tension. By cleaving (001) surfaces, new electronic features different from that of the bulk conformation are obtained. Specifically, MnNa-terminated surfaces exhibit a metallic nature regardless of the thickness. In contrast, a half-metallicity is observed for the As-terminated surfaces that is retained by varying the slab thickness. In all cases, Mn atoms mainly originate the magnetic moment, whose local value decreases slightly from inner to outside layers because of the stronger interactions with As atoms. In the case of As-termination, a small contribution from the outermost As layer is also noted that exhibits an antiparallel spin orientation with Mn atoms. PDOS spectra demonstrate that the electronic and magnetic properties of both bulk and (001) surfaces are determined by As-p and Mn-d states. Analyzing through the calculated magnetic anisotropy energy, the out-of-plane easy magnetizations are found for the half-metallic As-terminated surfaces with 5ML, 7ML, and 9ML thicknesses. Therefore these surfaces are highly recommended for application in spin injectors or the construction of magnetic spin junctions.

Data availability

Data will be provided upon request to the corresponding author.

Conflicts of interest

The authors declare that they have no known competing financial interests or personal relationships that could have appeared to influence the work reported in this paper.

Acknowledgements

ARS acknowledges the project PAPIIT-UNAM-IG101623.

References

1 A. Hirohata, K. Yamada, Y. Nakatani, I.-L. Prejbeanu, B. Diény, P. Pirro and B. Hillebrands, Review on spintronics: Principles and device applications, *J. Magn. Magn. Mater.*, 2020, **509**, 166711.
2 I. Žutić, J. Fabian and S. D. Sarma, Spintronics: Fundamentals and applications, *Rev. Mod. Phys.*, 2004, **76**(2), 323.
3 K. D. Belashchenko, J. K. Glasbrenner and A. L. Wysocki, Spin injection from a half-metal at finite temperatures, *Phys. Rev. B: Condens. Matter Mater. Phys.*, 2012, **86**(22), 224402.
4 G. De Wijs and R. De Groot, Towards 100% spin-polarized charge-injection: The half-metallic NiMnSb/CdS interface, *Phys. Rev. B: Condens. Matter Mater. Phys.*, 2001, **64**(2), 020402.
5 C. Hordequin, J. Nozieres and J. Pierre, Half metallic NiMnSb-based spin-valve structures, *J. Magn. Magn. Mater.*, 1998, **183**(1–2), 225–231.
6 J. Caballero, Y. Park, J. Childress, J. Bass, W.-C. Chiang, A. Reilly, W. Pratt Jr and F. Petroff, Magnetoresistance of NiMnSb-based multilayers and spin valves, *J. Vac. Sci. Technol., A*, 1998, **16**(3), 1801–1805.
7 W. Kim, K. Kawaguchi, N. Koshizaki, M. Sohma and T. Matsumoto, Fabrication and magnetoresistance of tunnel junctions using half-metallic Fe_3O_4, *J. Appl. Phys.*, 2003, **93**(10), 8032–8034.
8 Q. Lu, W.-J. Gong, S. Li, X.-T. Zu and H.-F. Lü, Half-metallic CrAs nanosheet for magnetic tunnel junctions, *Phys. Rev. Appl.*, 2024, **22**(2), 024002.
9 R. A. de Groot, F. M. Mueller, P. v. van Engen and K. Buschow, New class of materials: half-metallic ferromagnets, *Phys. Rev. Lett.*, 1983, **50**(25), 2024.
10 H. Akinaga, T. Manago and M. Shirai, Material design of half-metallic zinc-blende CrAs and the synthesis by molecular-beam epitaxy, *Jpn. J. Appl. Phys.*, 2000, **39**(11B), L1118.
11 G. Prathiba, S. Venkatesh, M. Rajagopalan and N. H. Kumar, Half metallic Co_2TiGe - a theoretical and experimental investigation, *J. Magn. Magn. Mater.*, 2011, **323**(1), 22–27.
12 H. Zhang, W. Liu, X. Dai, X. Zhang, H. Liu, X. Yu and G. Liu, Synthesis, structure, magnetic and half-metallic properties of $Co_{2-x}Ru_xMnSi$ (x= 0, 0.25, 0.5, 0.75, 1) compounds, *IUCrJ*, 2020, **7**(1), 113–120.
13 X. L. Wang, Proposal for a new class of materials: spin gapless semiconductors, *Phys. Rev. Lett.*, 2008, **100**(15), 156404.
14 Z. Yue, Z. Li, L. Sang and X. Wang, Spin-gapless semiconductors, *Small*, 2020, **16**(31), 1905155.
15 Y. Wang, X. Zhang, B. Ding, Z. Hou, E. Liu, Z. Liu, X. Xi, H. Zhang, G. Wu and W. Wang, Magnetic semiconductors based on quaternary Heusler compounds, *Comput. Mater. Sci.*, 2018, **150**, 321–324.
16 D. Hoat, D.-Q. Hoang, M. Naseri, J. Rivas-Silva, A. Kartamyshev and G. H. Cocoletzi, Computational prediction of the spin-polarized semiconductor equiatomic quaternary Heusler compound MnVZrP as a spin-filter, *RSC Adv.*, 2020, **10**(43), 25609–25617.
17 X. Wang, Z. Cheng, G. Zhang, H. Yuan, H. Chen and X.-L. Wang, Spin-gapless semiconductors for future spintronics and electronics, *Phys. Rep.*, 2020, **888**, 1–57.
18 W. Feng, X. Fu, C. Wan, Z. Yuan, X. Han, N. V. Quang and S. Cho, Spin gapless semiconductor like Ti_2MnAl film as a new candidate for spintronics application, *Phys. Status Solidi RRL*, 2015, **9**(11), 641–645.
19 H. Katayama-Yoshida and K. Sato, Spin and charge control method of ternary II–VI and III–V magnetic semiconductors for spintronics: Theory *vs*. experiment, *J. Phys. Chem. Solids*, 2003, **64**(9–10), 1447–1452.
20 A. Telegin and Y. Sukhorukov, Magnetic semiconductors as materials for spintronics, *Magnetochemistry*, 2022, **8**(12), 173.
21 T. Graf, C. Felser and S. S. Parkin, Simple rules for the understanding of Heusler compounds, *Prog. Solid State Chem.*, 2011, **39**(1), 1–50.
22 V. G. de Paula and M. S. Reis, All-d-metal full Heusler alloys: A novel class of functional materials, *Chem. Mater.*, 2021, **33**(14), 5483–5495.
23 I. Galanakis, P. Dederichs and N. Papanikolaou, Slater-Pauling behavior and origin of the half-metallicity of the full-Heusler alloys, *Phys. Rev. B: Condens. Matter Mater. Phys.*, 2002, **66**(17), 174429.
24 J. K. Kawasaki, S. Chatterjee, P. C. Canfield and G. Editors, Full and half-Heusler compounds, *MRS Bull.*, 2022, **47**(6), 555–558.
25 F. Casper, T. Graf, S. Chadov, B. Balke and C. Felser, Half-Heusler compounds: novel materials for energy and spintronic applications, *Semicond. Sci. Technol.*, 2012, **27**(6), 063001.
26 L. Bainsla, A. Mallick, M. M. Raja, A. Nigam, B. C. S. Varaprasad, Y. Takahashi, A. Alam, K. Suresh and K. Hono, Spin gapless semiconducting behavior in equiatomic quaternary CoFeMnSi Heusler alloy, *Phys. Rev. B: Condens. Matter Mater. Phys.*, 2015, **91**(10), 104408.
27 L. Bainsla and K. Suresh, Equiatomic quaternary Heusler alloys: A material perspective for spintronic applications, *Appl. Phys. Rev.*, 2016, **3**(3), 031101.
28 C. Felser, L. Wollmann, S. Chadov, G. H. Fecher and S. S. Parkin, Basics and prospective of magnetic Heusler compounds, *APL Mater.*, 2015, **3**(4), 041518.
29 K. Elphick, W. Frost, M. Samiepour, T. Kubota, K. Takanashi, H. Sukegawa, S. Mitani and A. Hirohata, Heusler alloys for spintronic devices: review on recent development and future perspectives, *Sci. Technol. Adv. Mater.*, 2021, **22**(1), 235–271.

30 S. Chadov, X. Qi, J. Kübler, G. H. Fecher, C. Felser and S. C. Zhang, Tunable multifunctional topological insulators in ternary Heusler compounds, *Nat. Mater.*, 2010, **9**(7), 541–545.

31 T. V. Vu, D. K. Nguyen, J. Guerrero-Sanchez, J. Rivas-Silva, G. H. Cocoletzi and D. Hoat, A new family of NaTMGe (TM= 3d transition metals) half-Heusler compounds: the role of TM modification, *RSC Adv.*, 2022, **12**(40), 26418–26427.

32 D. Hoat, M. Naseri, R. Ponce-Pérez, J. Rivas-Silva, A. Kartamyshev and G. H. Cocoletzi, P-substitution effects on the electronic structure and thermal properties of the half-metallic half-heusler NaCrBi compound, *Chem. Phys.*, 2020, **537**, 110848.

33 J. M. K. Al-zyadi, G. Gao and K.-L. Yao, First-principles investigation of the structural and electronic properties of bulk full-heusler alloy Mn_2CoSn and its (001) surface, *J. Alloys Compd.*, 2013, **565**, 17–21.

34 J. Li and Y. Jin, Half-metallicity of the inverse heusler alloy Mn_2CoAl (001) surface: A first-principles study, *Appl. Surf. Sci.*, 2013, **283**, 876–880.

35 W. Kohn and L. J. Sham, Self-consistent equations including exchange and correlation effects, *Phys. Rev.*, 1965, **140**(4A), A1133.

36 K. Schwarz and P. Blaha, Solid state calculations using WIEN2k, *Comput. Mater. Sci.*, 2003, **28**(2), 259–273.

37 J. P. Perdew, K. Burke and M. Ernzerhof, Generalized gradient approximation made simple, *Phys. Rev. Lett.*, 1996, **77**(18), 3865.

38 S. L. Dudarev, G. A. Botton, S. Y. Savrasov, C. Humphreys and A. P. Sutton, Electron-energy-loss spectra and the structural stability of nickel oxide: An LSDA+U study, *Phys. Rev. B: Condens. Matter Mater. Phys.*, 1998, **57**(3), 1505.

39 A. Ali, H. Elsaeedy, S. Ullah, S. A. Khan and I. Khan, First-principles study of polar magnets corundum double-oxides Mn_2FeMO_6 (M= W and Mo), *J. Magn. Magn. Mater.*, 2022, **563**, 169942.

40 S. Kervan and N. Kervan, First-principles study on half-metallic ferromagnetism in the diluted magnetic semiconductor (DMS) $Al_{1-x}Mn_xP$ compounds, *J. Magn. Magn. Mater.*, 2015, **382**, 63–70.

41 F. Birch, Finite strain isotherm and velocities for single-crystal and polycrystalline NaCl at high pressures and 300 K, *J. Geophys. Res.:Solid Earth*, 1978, **83**(B3), 1257–1268.

42 A. Togo and I. Tanaka, First principles phonon calculations in materials science, *Scr. Mater.*, 2015, **108**, 1–5.

43 I. Galanakis, P. Mavropoulos and P. H. Dederichs, Electronic structure and Slater–Pauling behaviour in half-metallic Heusler alloys calculated from first principles, *J. Phys. D: Appl. Phys.*, 2006, **39**(5), 765.

44 D. Rai, L. Fomin, I. Malikov, A. Sayede, M. P. Ghimire, R. Thapa, L. Zadeng, *et al.*, Pressure dependent half-metallic ferromagnetism in inverse Heusler alloy Fe_2CoAl: a DFT+U calculations, *RSC Adv.*, 2020, **10**(73), 44633–44640.

45 E. Şaşıoğlu, L. Sandratskii and P. Bruno, Above-room-temperature ferromagnetism in half-metallic Heusler compounds NiCrP, NiCrSe, NiCrTe, and NiVAs: A first-principles study, *J. Appl. Phys.*, 2005, **98**(6), 063523.

46 A. M. Mebed, M. Mushtaq, M. Faizan, R. Neffati, A. Laref, S. Godara and S. Maqbool, Adsorption of CO over the Heusler alloy CrCoIrGa (001) surface: first-principles insights, *RSC Adv.*, 2022, **12**(28), 17853–17863.

47 G. Gao and K. Yao, Half-metallic sp-electron ferromagnets in rocksalt structure: The case of SrC and BaC, *Appl. Phys. Lett.*, 2007, **91**(8), 082512.

48 G. Gao, L. Hu, K. Yao, B. Luo and N. Liu, Large half-metallic gaps in the quaternary Heusler alloys CoFeCrZ (*Z*= Al, Si, Ga, Ge): A first-principles study, *J. Alloys Compd.*, 2013, **551**, 539–543.

49 G.-X. Qian, R. M. Martin and D. Chadi, First-principles study of the atomic reconstructions and energies of Ga-and As-stabilized GaAs (100) surfaces, *Phys. Rev. B: Condens. Matter Mater. Phys.*, 1988, **38**(11), 7649.

50 M. G. Moreno-Armenta, J. Corbett, R. Ponce-Perez and J. Guerrero-Sanchez, A DFT study on the austenitic Ni_2MnGa (001) surfaces, *J. Alloys Compd.*, 2020, **836**, 155447.